https://erjm.journals.ekb.eg
ISSN: 1110-1180

DOI: ---------

ERJ
Engineering Research Journal
Faculty of Engineering
Menoufia University

Behavior of Space Trusses with CFST as Compression Elements

Mohamed I. Mousa[1*], Kamel A. Kandeel[2] and Maher M. Elabd[2]

[1]Civil Eng. Department, Higher Institute of Engineering and Technology in Kafr El-sheikh, Egypt.
[2] Civil Eng. Department, Faculty of Eng., Menoufia University, Shebin al-Kom, Egypt.
(Corresponding author: Mohamedrady202011@gmail.com)

ABSTRACT
Concrete Filled Tubular Steel (CFST) members are recently used widely due to their proved efficiency. CFST members can carry high axial compression forces which merge the advantages of steel and concrete sections. This paper presents an investigation for the use of CFST members as compression elements in space trusses through experimental and finite element (FE) modeling program. This program included two steps. The first step presents a comparison between hollow steel and CFST slender columns. The second step considers the behavior of full space truss with CFST members. The study also presents a FE modeling for all tested specimens (steel and CFST members). Test results like, ultimate load capacity, load against axial shortening and deformed mode shape are presented and discussed. The study reported the improvements that obtained by applying the technique of replacing the compression members in space trusses with CFST elements. The FE showed an excellent agreement with the experimental results.

Keywords: *steel, concrete, space truss, concrete filled tubular steel and finite element.*

1. Introduction

A space truss is a three-dimensional structural system composed of linear elements. It consists of two parallel grid layers of members (chord members) connected by vertical or diagonal members (web members). Circular steel pipes are the most popular cross-section for space truss elements. The need for efficient compression members led to the use of CFST members. This paper investigates composite trusses containing concrete-filled tubular steel members. Previous studies by Schmidt [1&2] examined three small-scale space trusses with edge supports and 6×6 panels measuring 1830×1830×216 mm overall. The study reported linear behavior until failure. El-Sheikh and McConnel [3] presented experimental loading test results on a corner-supported space truss measuring 4000 x 4000 mm with a depth of 575 mm, where buckling mode was the dominant failure mode that started on the upper chords. Fülöp and Iványi [4] presented experimental test results on the behavior of an N-type segment space truss with a 3 × 3 lower layer grid and a 2 × 2 upper layer grid, where theoretical length of grid bars and diagonals was 1200 mm; collapse occurred due to local buckling of two opposite diagonals at the top center joint. Kim et al. [5] showed the behavior of three different layout space trusses under vertical load until failure; failure mode shape occurred after reaching the ultimate load due to buckling in upper chord members. Sahol Hamid et al. [6] studied double-layer space truss behavior through finite element program; model results were compared with previous experimental tests and good agreement between experimental and FE results were obtained using ABAQUS.

Young & Ellobody [7] , Ellobody [8] and Ellobody [9] presented in their studies the behavior of concrete filled steel tubes. Also a comparison was drawn between the concrete filled steel tubes and empty tubes. Different parameters were discussed such as cross section shape, dimensions, length of specimen and concrete cylinder strengths varied. Also, FE analysis investigation was drawn on concrete filled stainless steel slender tube columns by the study presented the steps of CFST modeling and how to make a perfect modeling. Uy et. al. [10] investigated the behavior of slender CFST columns. The investigation was drawn through experimental program under axial loading. The study included 24 Specimens with different cross section shape: circular, square and rectangular. A total of 29 CFST columns with square section were investigated by Dundu [11]. The investigation was drawn through experimental tests. The load test was axial compression load till failure to study the ultimate load and failure shape mode.

Fong et al. [12] studied the effect of using CFST truss members and presented the load-carrying capacity and ductility of composite steel trusses compared to

hollow steel ones. Experimental results showed that the maximum load resisted by a member in the composite truss was 29% higher than that of the steel truss. Both steel and composite trusses had the same failure mode shape: overall buckling of compression members. Han et al. [13] presented experimental tests on CFST chords of steel trusses and compared the behavior of composite trusses with hollow tube steel trusses. Three CFST trusses and one steel truss were investigated; all had a span of 5000 mm and height of 485 mm. Chen et al. [14] investigated concrete-filled tubular steel trusses, including four circular hollow section tubular multi-planar trusses to ensure no lateral displacement occurred during testing; only top chords were in-filled with concrete.

Previous studies presented the behavior of concrete filled tubular steel as separate elements. also, few studies were drawn the using of CFST element on planer steel trusses. we can note, space truss studies were not included the using of CFST element. And so, the thesis will be discussing the behavior of space truss with CFST element. Thesis will present experimental tests and finite element investigation on CFST as sperate elements and as truss elements on space truss.

2. Experimental Investigation

The experimental program consists of two series. The first series includes 12 separate slender column specimens divided into two groups: 6 hollow steel columns and 6 CFST columns. The second series includes 4 space truss models with the same configurations; two trusses have hollow steel tube elements while the other two have their upper chord members replaced with CFST members. All steel tubes had a yield stress of 440 MPa and self-compacting concrete with a compressive strength of 35 MPa was used to fill the steel tubes.

Trial mixes were carried out using the absolute volume method to design the concrete mixes used in this study. Table (1) shows mixes designed using this method and materials mentioned earlier. A total of three standard 150 mm cubes were prepared from this mix and tested after 28 days of casting. The results were carried out using the compression testing machine. for the steel tubes and plates, the slices were taken and tested up using direct tensile test.

2.1 Sperate Slender Column Tests.

The two groups of columns had the same steel tube properties, as shown in Table (2). Column specimens were made from circular steel tubes with three different diameters: 42.0 mm, 48.8 mm, and 60.30 mm; tube wall thicknesses were 3.00 mm, 2.80 mm, and 3.00 m, respectively. Specimen lengths were 1000 mm and 1250 mm. Figure (1) shows one of the column specimens.

Specimens were labeled according to whether they were steel columns (SC) or composite columns (CC). The third and fourth letters indicated their nominal diameter: 42 for 42.00 mm, 48 for 48.80 mm and 60 for 60.30 mm while the fifth letter (L) indicated their length in meters. For example, specimen CC60L1.25 was a concrete-filled tubular column with a diameter of 60.30 mm and length of 1250mm.

Table 1 - Trial Self- Compacted Concrete Mix

Cement content (kg)	Coarse Aggregate content (kg)	Sand content (kg)	Water content (kg)	ADDICRETE BVF Content (kg)
400	1150	595	200	6

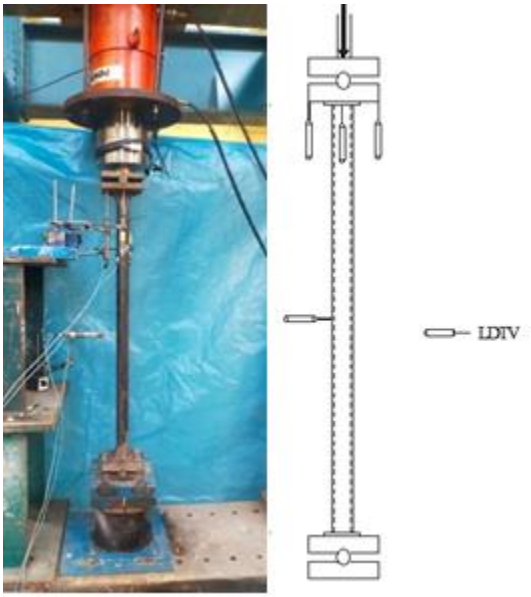

Figure 1–Photo of Separate specimens and Test set up and locations of LDTVs

2.2 Test Setup and Instrumentation of Sperate slender column tests

All columns were tested using a loading jack with a maximum capacity of 1000 kN. Specimens were subjected to axial force at the top of the columns with a load interval of 2 kN throughout the test. A load cell was located at the top of the specimen to record applied load, as shown in Figure (1). A rigid 50 mm-thick plate was placed under the loading jack and another at the bottom of specimens as support; a tie-rod was placed between plates to allow rotation in one direction, see Figure (1). Column boundary conditions were pinned in-plan direction; rotation in this direction was permissible while out-of-plan rotation was prevented. Four displacement transducers (LDTV) were used and placed at the middle and top of the

column; all LDTVs were connected to a data logger to display axial displacement and mid-span deflection.
The tests on separate elements were drawn to calculate the ultimate load capacity and deformed shapes and measure the effect of using concrete on steel tubes members.

Table 2 –Properties and Dimension of Specimens of the First Series`

Specimen Label	Dimensions					Concrete Strength F_{cu} (MPa)	Steel Strength F_y (MPa)
	D(mm)	t(mm)	L(mm)	D/t	$\lambda = L_e / r$		
SC42L1.00	42.00	3.00	1000	14.06	76.98	-----	295
SC42L1.25	42.00	3.00	1250	14.06	94.98	-----	295
SC48L1.00	48.80	2.80	1000	17.14	66.83	-----	295
SC48L1.25	48.80	2.80	1250	17.14	82.44	-----	295
SC60L1.00	60.30	3.00	1000	20.10	52.74	----	295
SC60L1.25	60.30	3.00	1250	20.10	65.07	----	295
CC42L1.00	42.00	3.00	1000	14.06	76.98	35	295
CC42L1.25	42.00	3.00	1250	14.06	94.98	35	295
CC48L1.00	48.80	2.80	1000	17.14	66.83	35	295
CC48L1.25	48.80	2.80	1250	17.14	82.44	35	295
CC60L1.00	60.30	3.00	1000	20.10	52.74	35	295
CC60L1.25	60.30	3.00	1250	20.10	65.07	35	295

2.3 Space Trusses Tests.

Space truss specimens were divided into two groups: the first group included two space trusses with hollow pipes while the second group included two composite space trusses. All four space trusses measured 3840 mm in length, 1280 mm in width and 900 mm in height, see Figure (2). Space truss members were made of circular hollow sections with equal lengths of 1000 mm and consisted of 3x1 panels; each panel was square-shaped and measured 1280 x 1280 mm. Two different cross-sections were selected for top chord members: CHS42.0x3 for the first space truss and CHS48.8X2.8 for the second; all lower and diagonal members had cross-section CHS60.3x3.2 for all truss specimens. Composite steel truss members were filled with self-compacting concrete with compression strength of 35 MPa, see Table (3). Four space trusses were made: two with hollow steel tubular elements and two with hollow steel elements except upper chord members made of CFST elements. ST1 and CT1 trusses had identical configurations regarding dimensions of truss members; using CFST elements instead of hollow tubular elements for upper chords was the only difference between ST1, ST2 and CT1, CT2.
All space trusses were design and manufactured as simple truss. the configuration of supports was hinged for three supports and the fourth support was roller. The connection between members was pin type. Members were connected using a guest plate with a thickness of 10 mm and one bolt with a diameter of 24 mm and grade 10.9. Two welding joints were selected to prepare space trusses: tee joint and corner joint using maximum allowable weld size equal to 70% of plate thickness.

2.4 Test Setup and Instrumentation of Space Trusses Tests.

All space trusses were tested to failure and subjected to static load at the middle joint in the upper chord of the truss. Four LDVTs were used and fixed to measure the horizontal displacement and deflection, see Figure (3). LDVT 1 and 2 were fixed at the middle length of lower mesh members and measured overall space truss deflection. LDVT 3 and 4 were fixed at the left member of upper chord; LDVT 3 measured in-plan displacement while LDVT 4 measured out-of-plan displacement.

Table 3–Experimental Load Capacity of Slender Column Specimens.

Specimen Label	Upper Mesh Section	Lower Mesh & Diagonal Section	Concrete Strength F_{cu} (MPa)	Steel Strength F_y (MPa)
ST1	CHS42.0x3.0	CHS60.3x3.0	------	295
ST2	CHS48.8x2.8	CHS60.3x3.0	------	295
CT1	CHS42.0x3.0	CHS60.3x3.0	35	295
CT2	CHS48.8x2.8	CHS60.3x3.0	35	295

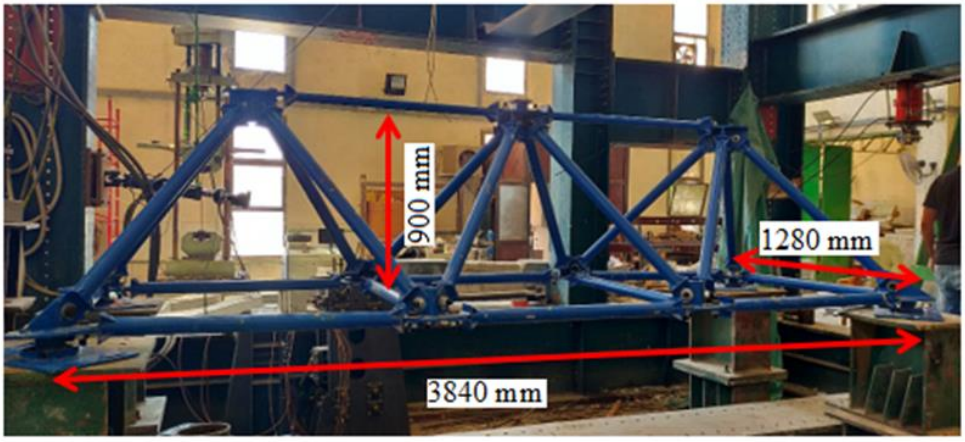

Figure 2– Photo and Layout Dimension of Space Truss

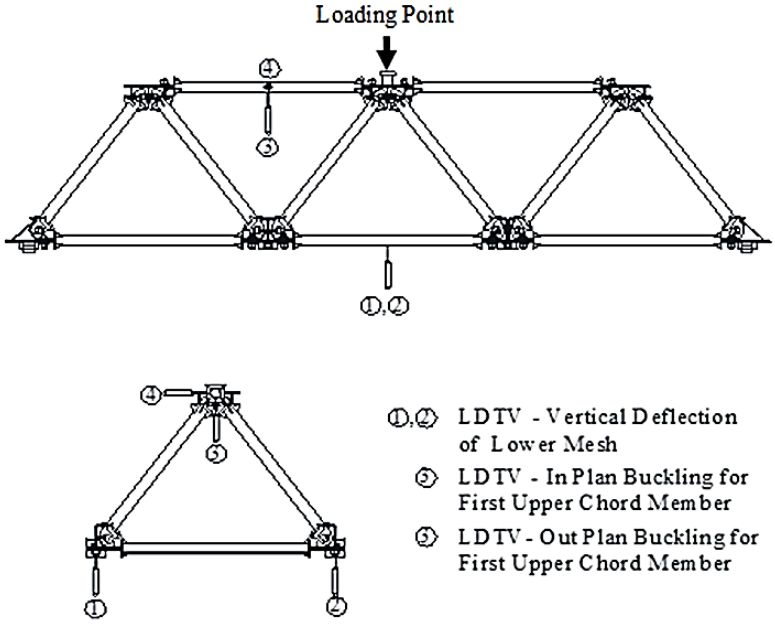

Figure 3– Sketch of Space Truss Specimens Under Testing.

3. Results of Sperate Slender Column Tests.

3.1 Ultimate Load Capacity

Column load-carrying capacity ($P_{Exp.}$) was measured by determining peak load from experimental tests. Tests began with regular 5.0 kN increments up to maximum load; peak load was the maximum load resisted by the column. Failure loads for all specimens were recorded to study the effect of buckling ratio. Comparisons were made between concrete-filled tubular columns and hollow steel columns; Table (4) presents experimental load capacity for each specimen.

Table 4 – Experimental Load Capacity of Slender Column Specimens

Specimen Label	Dimensions			Concrete Strength F_{cu} (MPa)	Steel Strength F_y (MPa)	P_{Exp} (kN)
	D (mm)	t (mm)	L(mm)			
SC42L1.00	42.00	3.00	1000	-----	295	99.51
SC42L1.25	42.00	3.00	1250	-----	295	89.40
SC48L1.00	48.80	2.80	1000	-----	295	121.20
SC48L1.25	48.80	2.80	1250	-----	295	114.30
SC60L1.00	60.30	3.00	1000	----	295	184.60
SC60L1.25	60.30	3.00	1250	----	295	174.40
CC42L1.00	42.00	3.00	1000	35	295	110.65
CC42L1.25	42.00	3.00	1250	35	295	97.90
CC48L1.00	48.80	2.80	1000	35	295	145.35
CC48L1.25	48.80	2.80	1250	35	295	136.70
CC60L1.00	60.30	3.00	1000	35	295	262.15
CC60L1.25	60.30	3.00	1250	35	295	246.15

3.2 Deformed Shape and Failure Mode

Load against axial shortening relations for column specimens is presented in Figures (4, 5 and 6). Curves were divided into three stages: elastic stage, elastic-plastic stage and plastic (post-ultimate) stage. The plastic or post-ultimate stage began with the peak load carried by the column up to failure; a rapid increase in axial displacement was noticed with a progressive drop in load. Figure (7) presents failure mode shapes of column specimens after tests; two deformed shapes were likely to occur: local buckling of steel tubes or overall buckling.

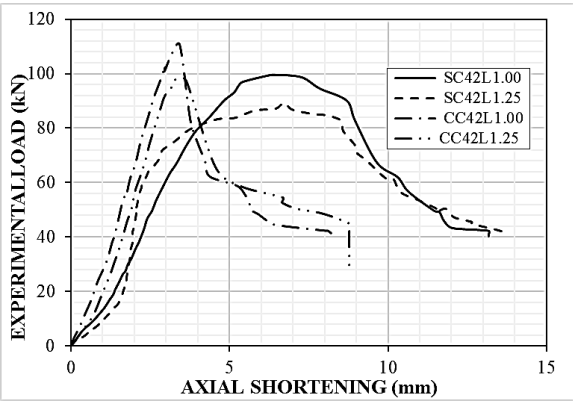

Figure 4– Experimental Load Against Axial Shortening Relation for SC42L1.00, SC42L1.25, CC42L1.00 And CC42L1.25.

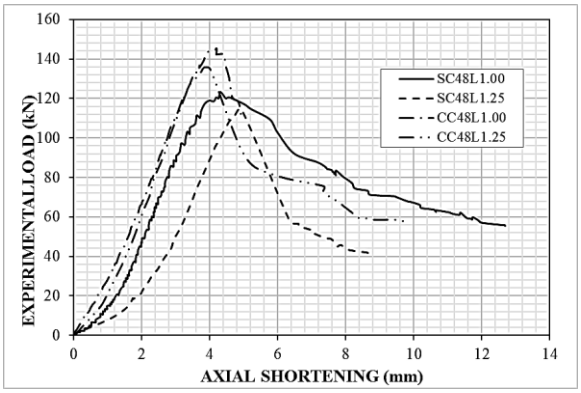

Figure 5– Experimental Load Against Axial Shortening Relation for SC48L1.00, SC48L1.25, CC48L1.00 and CC48L1.25.

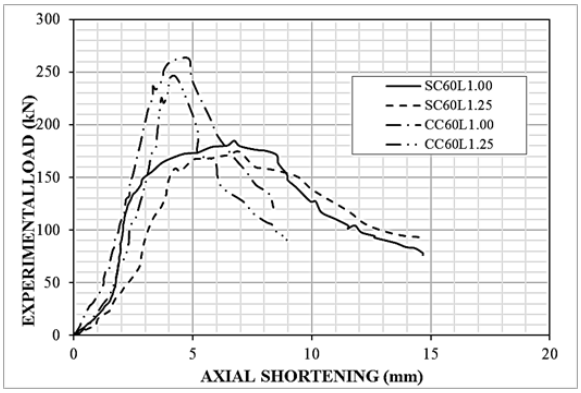

Figure 6 – Experimental Load Against Axial Shortening Relation for SC48L1.00, SC48L1.25, CC48L1.00 and CC48L1.25.

a) SC42L1.00 b) SC48L1.00 c) SC48L1.25 d) SC60L1.00 e) SC60L1.25

f) CC42L1.00 g) CC42L1.25 h) CC48L1.00 i) CC60L1.00 j) CC60L1.25

Figure 7 – Experimental failure mode shape for slender column specimens.

4. Results of Space Truss Tests.

4.1 Ultimate Load Capacity.

Table (5) presents ultimate or failure loads for four space trusses. Specimens ST1 and ST2 were space trusses with different upper chord sections; failure loads were 132.87 kN and 154.22 kN, respectively. Composite space trusses CT1 and CT2 with upper chord cross-sections CHS42.0x3.0 and CHS48.8x2.8 had failure loads of 145.54 kN and 186.25 kN, respectively.

4.2 Deformed Shape and Failure Mode

For space trusses, deflection at middle span was recorded during tests with increasing applied load. Figure (8) shows the relation between experimental applied load and deflection at middle span. The area under curves can be divided into two regions: the first region starts from test beginning up to ultimate load capacity where load and deflection increase together in a semi-linear relationship; the second region starts at ultimate load capacity and continues to test end up to failure where applied load decreases with significant increase in deflection. In general, steel space truss failure was brittle or compression failure.

Figures (9 to 12) show failure mode shapes of space truss specimens. Failure mode shape indicates space truss failure mode; all steel trusses were designed for top chord members to collapse under compression failure. Figure 9 presents failure mode shape of steel space truss ST1: at test beginning, space truss failed as one unit to reach ultimate load and left upper chord member rapidly buckled in-plan. Figure (9) shows that space truss ST1 failed in compression failure occurring at upper chords

Figure (10) shows failure mode shape of steel space truss ST2; truss CT1 had similar behavior to space truss ST1 except that right upper chord member buckled upon reaching ultimate load.

Figures (11 and 12) present failure mode shapes of composite space trusses CT1 and CT2; composite

truss behavior was similar to steel trusses with hollow pipes and failed due to collapse of right upper chord member. In general, all composite and non-composite space trusses collapsed under compression failure of upper chord members.

Table 5 – Experimental Load Capacity of Space Truss Specimens.

Specimen Label	Truss Type	Upper Mesh Section	Lower Mesh & Diagonal Section	Concrete Strength F_{cu} (MPa)	Steel Strength F_y (MPa)	Failure Load P_{Exp} (kN)
ST1	Steel	CHS42.0x3.0	CHS60.3x3.0	------	295	132.87
ST2	Steel	CHS48.8x2.8	CHS60.3x3.0	------	295	154.22
CT1	Composite	CHS42.0x3.0	CHS60.3x3.0	35	295	145 .54
CT2	Composite	CHS48.8x2.8	CHS60.3x3.0	35	295	186.25

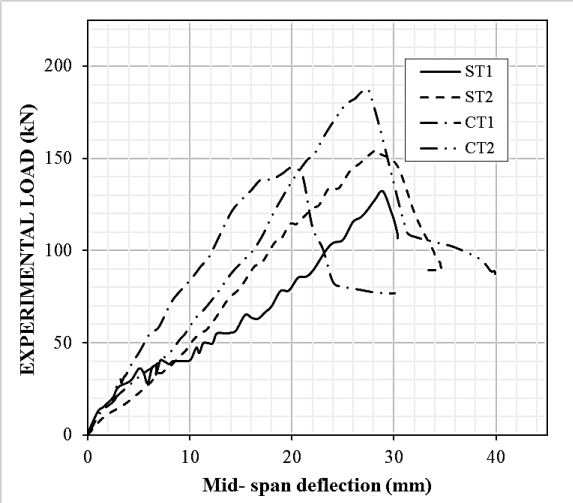

Figure 8 – Experimental Load Against Middle Span Deflection Relation for Space Trusses ST1, ST2, CT1 And CT2.

5. Finite Element (FE) Modeling and Validation

The current study presents an accurate finite element model for CFST and hollow tube steel members using ABAQUS 2017 [15] software program; results showed excellent agreement for linear and nonlinear analysis. Finite Element Modeling included identification of element part, mesh and material property as well as analysis type. Boundary condition, contact between element parts and load application were also included. Steel tubes were modeled as shell elements with reduced integration S4R while concrete-filled cores were modeled using 3-D solid C3D8. Hollow steel tube members were modeled as shell or wire elements. For CFST columns, all degrees of freedom for top and bottom surfaces were prevented except displacement at loaded end allowed in applied load direction. Load was applied as static uniform at upper rigid plate identical to experimental loading procedure. Tested space trusses were supported at four lower corners using pin supports; the first support was prevented from moving in all directions while the second support was allowed to move in X-direction and prevented in other two (Y + Z) axes; the third support was allowed to move only in Y-direction while the fourth support was allowed to move in all directions except Z-direction ,see Figure (13).

Several mesh sizes were tried to achieve reasonable mesh that provided reliable results while reducing computational time. It was found that a mesh size ratio of 1 (length): 1 (width): 2 (depth) for most elements achieved accurate results.

The connection between the wire parts was simulated as hinge which was created automatically. The option of coupling was selected for the connection between the shell or solid and wire parts. The meeting joint of parts was selected to create the coupling as master constraint. Then select the shell or solid part surface as slave.

5.1 Material Modeling of The Normal Confined Concrete and Steel Tube.

To model the concrete core, a procedure similar to that presented by Ellobody and Young [7] was used. Figure (14) illustrates the relationship between the equivalent uniaxial stress-strain curves for both unconfined and confined concrete. The plastic part of the concrete was modeled using the DRUCKER PRAGER model available in ABAQUS [15]. Two parameters (*DRUCKER PRAGER and *DRUCKER PRAGER HARDENING) were used to define the yield stage of confined concrete. The material angle of friction (b) and the ratio of flow stress in tri-axial tension to that in compression (K) were taken as 20° and 0.8 respectively, as recommended by Hu et al. [16].

For modeling steel material, elastic properties were completely defined by providing Young's modulus (E) and Poisson's ratio (ν). The nonlinear part of steel material's stress-strain curve was modeled using the PLASTIC option available in ABAQUS [15], Mander

et al [17]. Contact elements were used to model interaction between internal surface of steel tube and external surface of concrete core. Coefficient of friction between two faces was taken as 0.25 for analysis. Interface element allows surfaces to separate under tensile force influence but prevents penetration through hard contact interface.

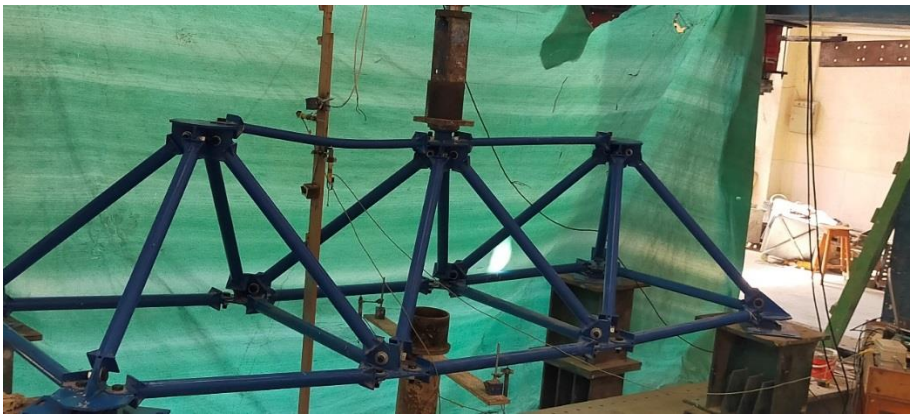

Figure 9 – Failure Mode Shape of Steel Space Truss ST1.

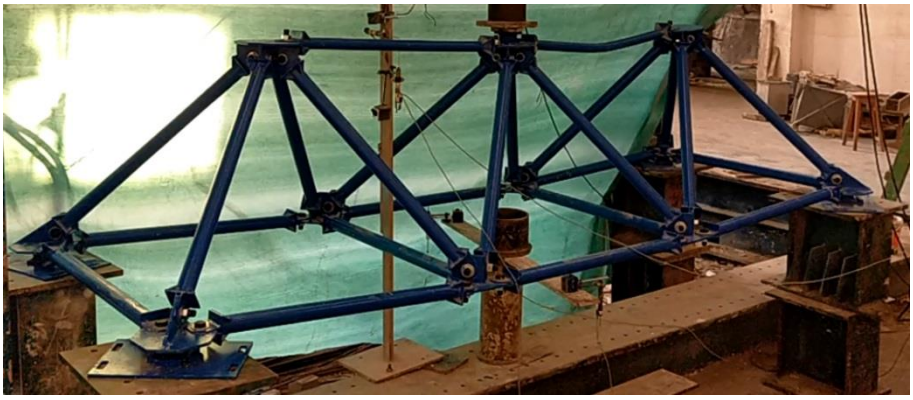

Figure 10 – Failure Mode Shape of Steel Space Truss ST2.

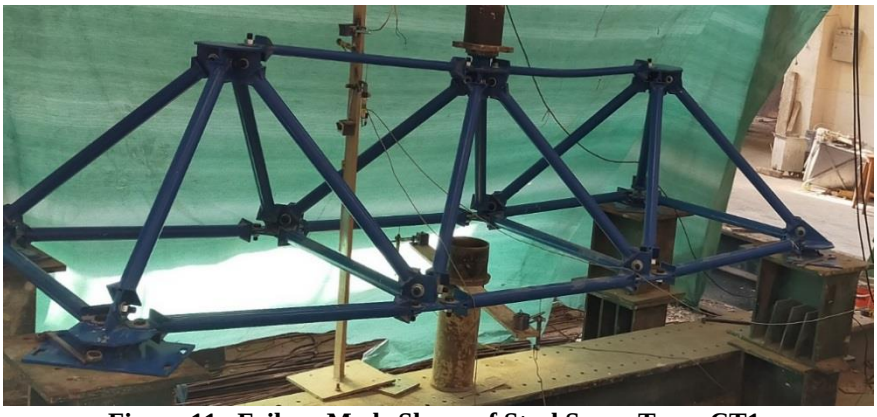

Figure 11– Failure Mode Shape of Steel Space Truss CT1.

Figure 12– Failure Mode Shape of Steel Space Truss CT2.

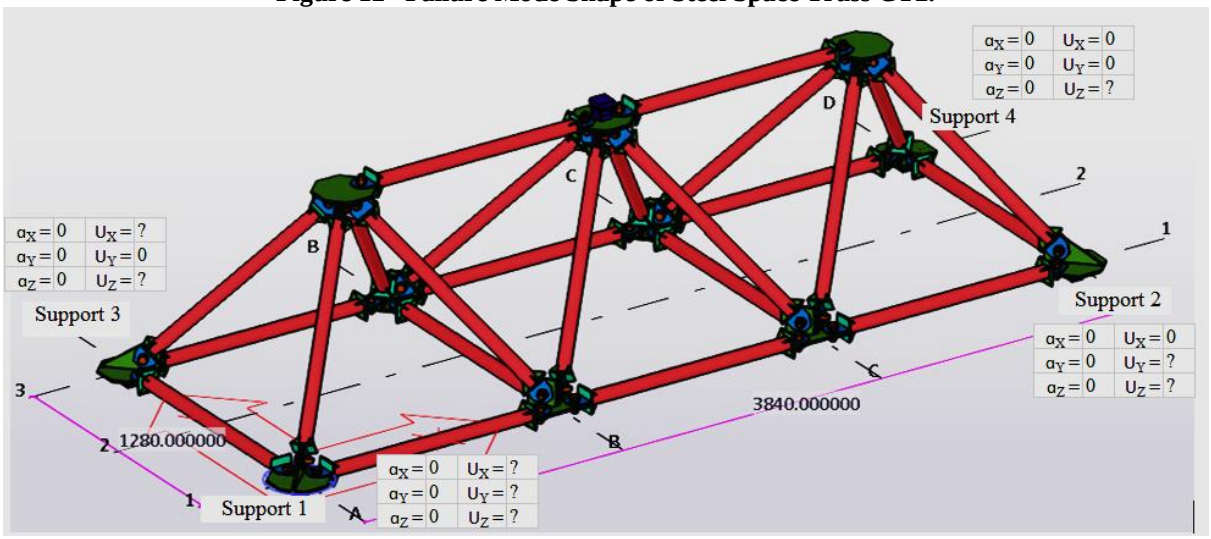

Figure 13 – Degree of Freedom for Experimental and Finite Element Modelling Space Trusses.

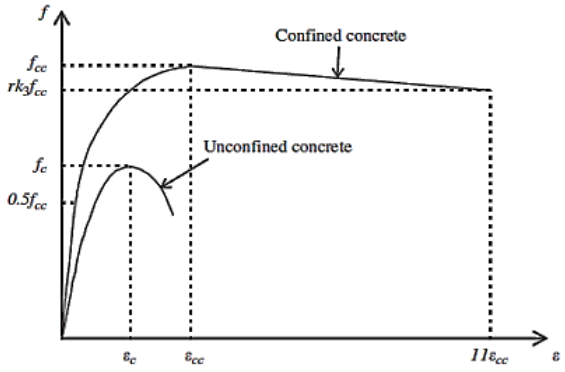

Figure 14 – Equivalent Uniaxial Stress–Strain Curves for Confined and Unconfined Concrete [16]

5.2 Proposed FE Models Results

Table (2) and Table (3) summarize the results of experimental tests for separate columns and space trusses, respectively. The same specimens were modeled using the ABAQUS finite element program. Results such as load-carrying capacity, load versus axial shortening, middle length deflection curves, and failure mode shape were extracted and explained from the finite element program. Finally, a validation process was performed to compare experimental and finite element results to ensure the accuracy of the finite element program.

5.3 Validation of Results for Slender Columns.

5.3.1 Load Carrying Capacity

Table (6) presents a comparison of ultimate load capacity between experimental and finite element results for individual specimens. The mean difference ratio between experimental and FE results was 7.49%, with the highest and lowest values being 9.10% and 4.26%, respectively.

2.3.1 Deformed shape and failure mode

Figures (15 to 20) present the experimental and FE modeling load axial shortening curves for all column specimens. Excellent agreement between finite element results and experimental results is observed except for specimens CC60L1.00 and CC60L1.25.

Table 6– Experimental and Finite Element Load Capacity of Slender Column Specimens.

Specimen Label	Dimensions			F_{cu} (MPa)	F_y (MPa)	P_{Exp} (kN)	$P_{F.E.}$ (kN)	difference ratio %
	D (mm)	t (mm)	L (mm)					
SC42L1.00	42.00	3.00	1000	-----	295	99.51	90.8	8.74
SC42L1.25	42.00	3.00	1250	-----	295	89.40	82.8	7.38
SC48L1.00	48.80	2.80	1000	-----	295	121.20	112.5	7.18
SC48L1.25	48.80	2.80	1250	-----	295	114.30	104.11	8.68
SC60L1.00	60.30	3.00	1000	----	295	184.60	167.8	9.10
SC60L1.25	60.30	3.00	1250	----	295	174.40	160	8.05
CC42L1.00	42.00	3.00	1000	35	295	110.65	101.5	8.23
CC42L1.25	42.00	3.00	1250	35	295	97.90	91	7.14
CC48L1.00	48.80	2.80	1000	35	295	145.35	139.1	4.27
CC48L1.25	48.80	2.80	1250	35	295	136.70	126.6	6.64
CC60L1.00	60.30	3.00	1000	35	295	262.15	239.7	8.51
CC60L1.25	60.30	3.00	1250	35	295	246.15	231.1	6.06

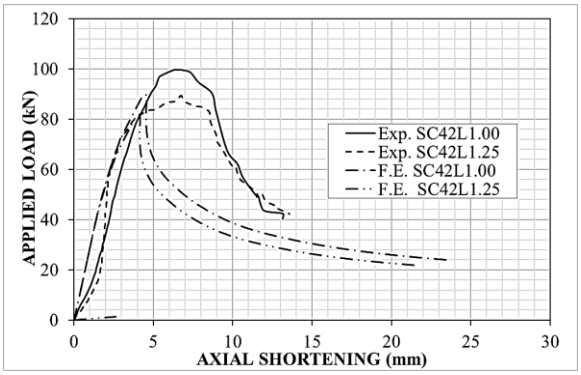

Figure 15 – Experimental and F.E. Modelling Load-Axial Shortening Curves for SC42L1.00 And SC42L1.25.

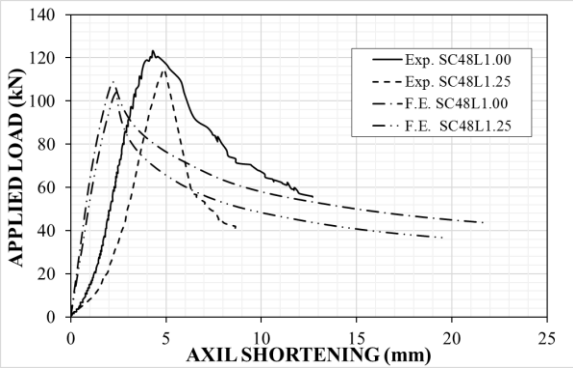

Figure16 – Experimental and F.E. Modelling Load-Axial Shortening Curves for SC48L1.00 And SC48L1.25.

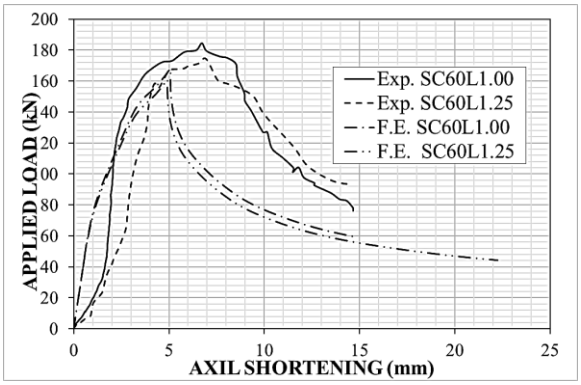

Figure 17 – Experimental and F.E. Modelling Load-Axial Shortening Curves for SC60L1.00 And SC60L1.25.

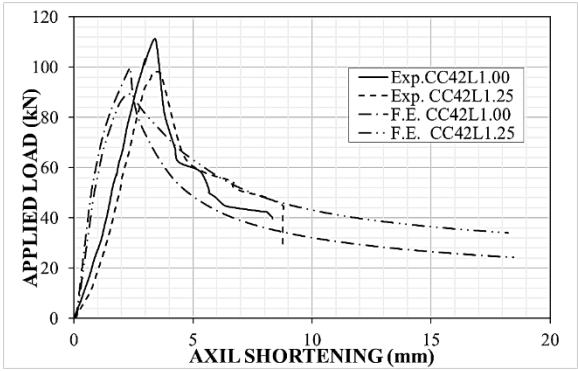

Figure 18–Experimental and F.E. Modelling Load-Axial Shortening Curves for CC42L1.00 And CC42L1.25.

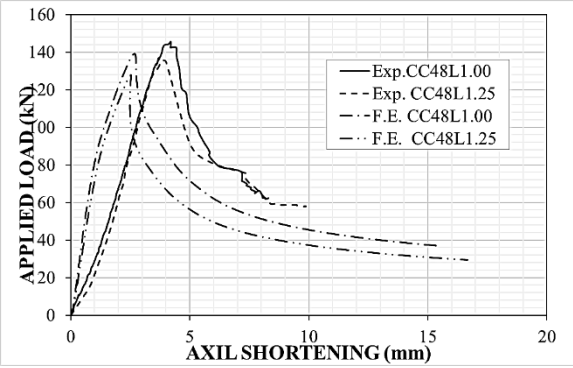

Figure 19 – Experimental and F.E. Modelling Load-Axial Shortening Curves for CC48L1.00 And CC48L1.25.

The finite element results for CC60L1.00 and CC60L1.25 were larger than those obtained from experimental results in terms of axial shortening versus ultimate load. In general, the behavior of finite element curves can be divided into three regions: elastic, elastic-plastic, and plastic.

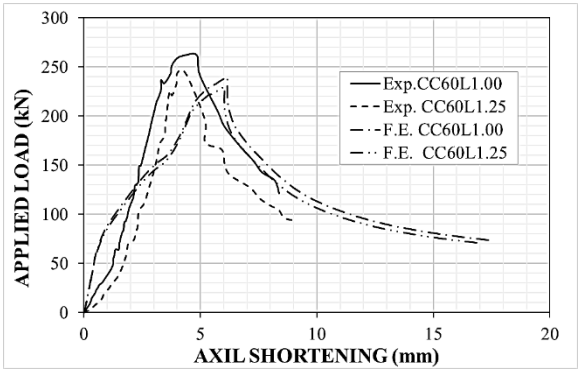

Figure 20 – Experimental and F.E. Modelling Load-Axial Shortening Curves for CC60L1.00 And CC60L1.25.

Figure (21) presents the deformed shape at failure from experimental tests and FE modeling for separate column specimens. The comparison clearly demonstrates the capabilities of FE modeling in simulating experimental tests. It is worth mentioning that all specimens failed due to overall buckling.

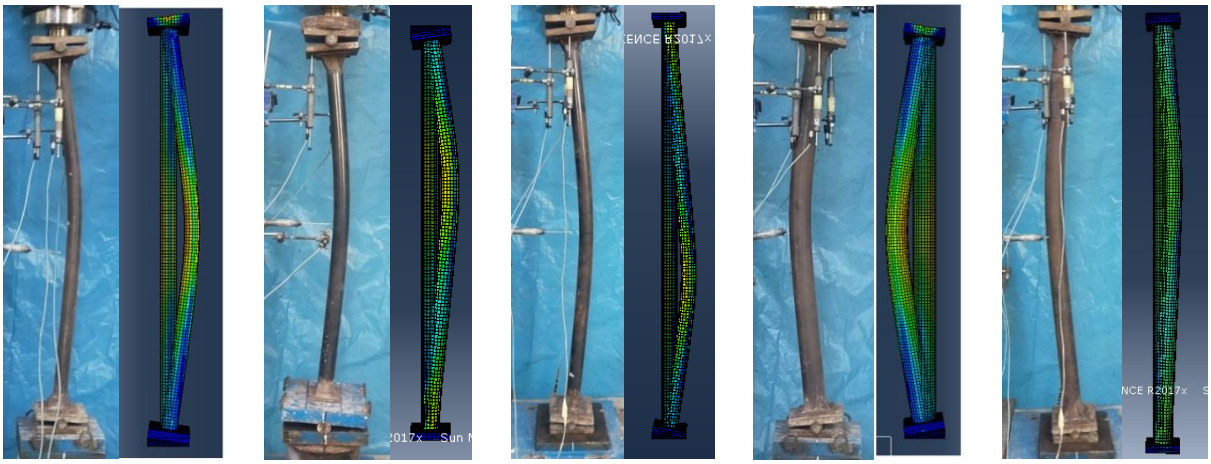

a) SC42L1.00 b) SC48L1.00 c) SC48L1.25 d) SC60L1.00 e) SC60L1.25

f) CC42L1.00 g) CC42L1.25 h) CC48L1.00 i) CC60L1.00 j) CC60L1.25

Figure 21 – Experimental and F.E. Modelling Failure Mode Shape for Slender Column Specimens.

5.4 Validation of Results for Space Trusses.

5.4.1 Load Carrying Capacity

Table (7) presents experimental and FE modeling results for four space truss models. The mean difference ratio between experimental and FE results was 7.49%, with the highest and lowest values being 9.10% and 4.26% respectively.

5.4.2 Deformed Shape and Failure Mode

Figures (22) and (23) present the load against mid-span deflection results obtained from FE modeling and experimental tests for steel and composite space trusses respectively. Generally, it can be observed that the FE modeling curves are divided into two regions. The first region starts at the beginning of the test until reaching ultimate load. In this region, load and deflection increase together in a semi-linear relationship. The second region starts at ultimate load to end of testing where load decreases with rapid increase in deflection for CT1 and CT2. The curves from FE modeling and experimental tests were largely identical. However, deflection from finite element modeling was observed to be less than that obtained from experimental tests. This behavior is expected to be due to clearances in bolt holes leading to additional slippage in connections.

Figures (24) to (27) show good agreement between failure modes, ultimate load capacity, and deformations that occurred during experimental tests and FE analysis for space trusses ST1, ST2 and CT2. It can also be observed that the dominant failure mode for all space trusses was compression failure in the upper chord member. From the discussion, it is clear that there is good agreement between FE modeling and experimental test results.

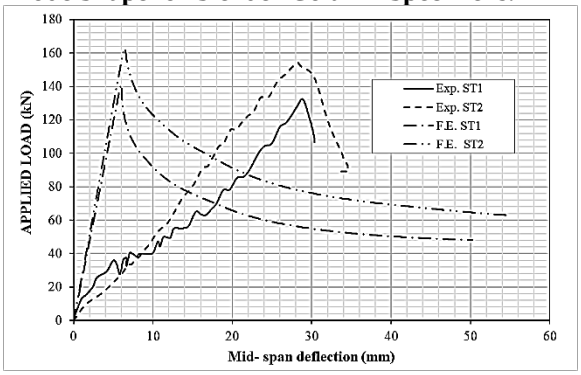

Figure 22 – Experimental and F.E. Modelling Load- Middle Span Deflection Curves for ST1 And ST2.

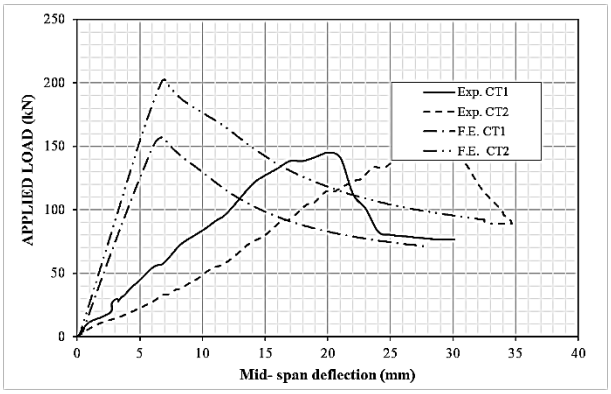

Figure 23 – Experimental and F.E. Modelling Load- Middle Span Deflection Curves for CT1 And CT2.

Table 7–Experimental and FE Modeling Load Capacity of Space Truss Specimens.

Specimen Label	Truss Type	Upper Mesh Section	Lower Mesh & Diagonal Section	F_{cu} (MPa)	F_y (MPa)	P_{Exp} (kN)	$P_{F.E.}$ (kN)	Difference ratio %
ST1	Steel	CHS42.0x3.0	CHS60.3x3.0	------	295	132.87	141.13	6.22
ST2		CHS48.8x2.8		------	295	154.22	162.89	5.63
CT1	Composite	CHS42.0x3.0		35	295	145 .54	157.25	8.05
CT2		CHS48.8x2.8		35	295	186.25	202.56	8.76

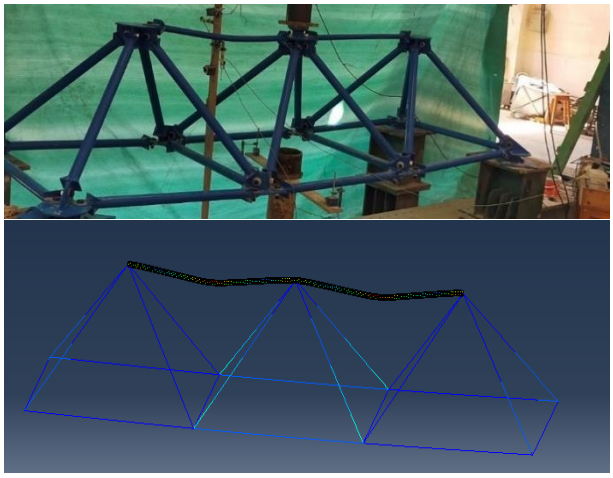

Figure 24 – F.E. Modelling and Experimental Deformed Shape of Steel Space Truss ST1.

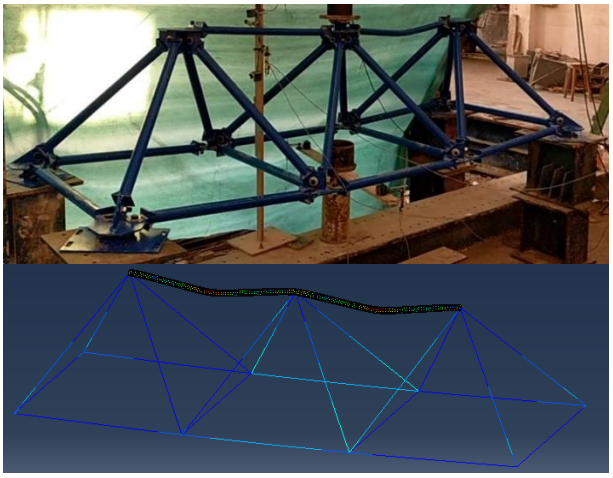

Figure 25 – F.E. Modelling and Experimental Deformed Shape of Steel Space Truss ST2.

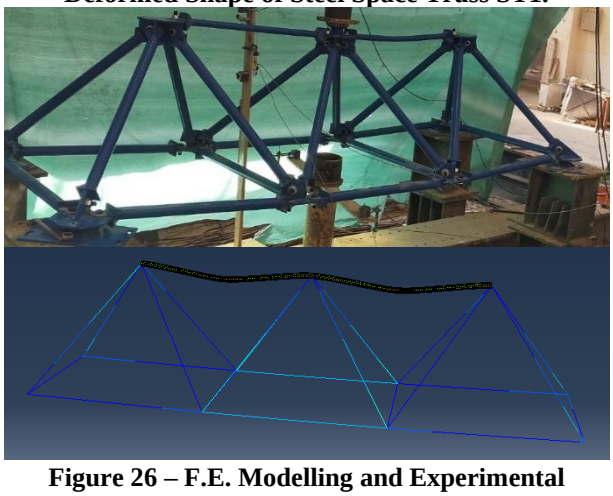

Figure 26 – F.E. Modelling and Experimental Deformed Shape of Steel Space Truss CT1.

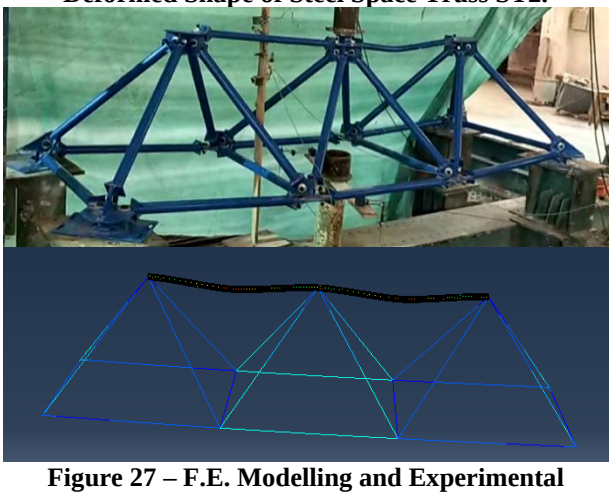

Figure 27 – F.E. Modelling and Experimental Deformed Shape of Steel Space Truss CT2.

6. Discussion of Results

Tables (8) and (9) present the ratio of load capacity increase for experimental test results for hollow tubes and CFST members as individual elements and for space trusses with hollow and CFST elements,

respectively. Six steel specimens with three different cross-sections were tested as individual elements. An increase ranging from 9.51% to 19.60% was recorded for individual CFST elements compared to hollow steel elements. A 9.54% increase was recorded for space truss CT1 with CFST composite elements compared to ST1 with non-composite elements. For second space truss T2, the ratio of ultimate load increase was 20.77% compared to steel truss ST2.

Figures (4) to (6) show comparisons between CFST and steel tubular specimens in terms of load against axial shortening curves. Each figure contains four curves: two for CFST and two for hollow steel elements. The curves in each figure are for steel tubes with the same diameter. From Figures (4) to (6), it can be observed that hollow steel columns are more ductile than concrete-filled steel tubular members.

Table 8–Comparison of Ultimate Load Capacity Between Steel and CFST Slender Column Specimens

SPECIMEN Label	Ultimate Load (kN)		Ratio of increase (%)
	CFST Column	Steel Column	
C42L1.00	110.65	99.51	11.19
C42L1.25	97.9	89.4	9.51
C48L1.00	145.35	121.2	19.93
C48L1.25	136.7	114.3	19.60
C60L1.00	262.15	184.6	42.01
C60L1.25	246.15	174.4	41.14

Table 9–Comparison of Ultimate Load Capacity Between Steel and Composite Trusses Specimens.

Specimen Label	Ultimate Load (kN)		Ratio of increase (%)
	Composite Truss	Steel Truss	
T1	145.54	132.87	9.54
T2	186.25	154.22	20.77

Figure (8) presents the applied load against deflection at mid-span for space truss specimens. Four curves are included: two for ST1 and ST2 which are steel space trusses and two for CT1 and CT2 which are space trusses with CFST members. The ductility of composite space trusses is less than that of steel ones. In general, all steel and composite trusses failed due to compression failure. The applied load on the truss increased linearly until reaching ultimate load then sudden collapse occurred.

The diameter-to-thickness (D/t) ratio of a steel tube is an important factor in selecting the tube. The D/t ratio has a significant effect on slenderness ratio as well as confinement pressure of the steel tube and concrete core. Therefore, the D/t ratio is considered along with the ratio of load capacity increase of concrete-filled steel compared to hollow steel tubular elements.

The first series of experimental programs includes six individual CFST elements with three different D/t ratios: 14.06, 17.14, and 20.1, respectively. Figures (28) and (29) present the relationship between diameter-to-thickness (D/t) ratio and Ratio of increase in ultimate load for individual CFST elements.

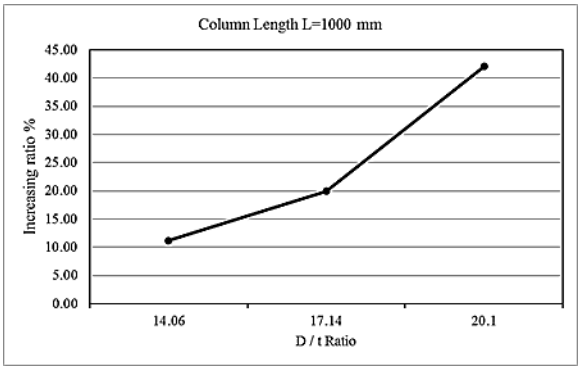

Figure 28 – Relation of Diameter to Thickness Ratio (D/T) And Ratio of Increase of Ultimate Load For CFST Columns CC42L1.00, CC48L1.00 And CC60L1.00

For column specimens with length 1000 mm, Figure 28 shows the relationship between D/t ratio and Ratio of increase in ultimate load capacity. The D/t ratio has a large effect on Ratio of increase in ultimate load capacity for CFST columns; increasing D/t ratio led to an increase in Ratio of increase in ultimate load capacity.

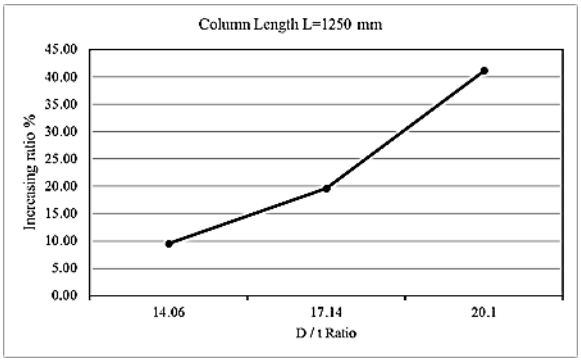

Figure 29 – Relation of Diameter to Thickness Ratio (D/T) and Ratio of Increase of Ultimate Load for CFST Columns CC42L1.25, CC48L1.25 And CC60L1.25.

The D/t ratios for CFST elements CT1 and CT2 are 14.06 and 17.14, respectively. Figure (30) shows the relationship between D/t ratio and Ratio of increase in ultimate load for composite space trusses. From Figure (30), it can be clearly observed that increasing D/t ratio led to an increase in ultimate load.

In general, the D/t ratio is an important parameter that has a significant effect on the ultimate load of CFST elements. The D/t ratio of steel tube influences confinement pressure of steel tube and concrete core.

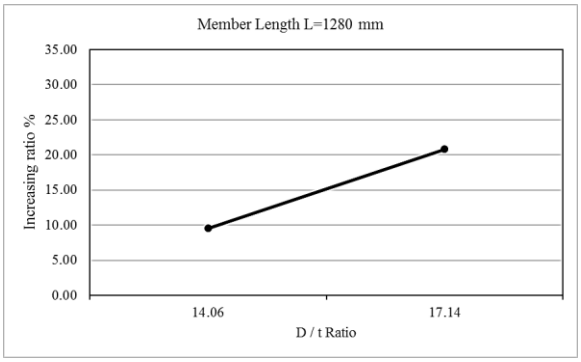

Figure 30 – Relation of Diameter to Thickness Ratio (D/T) and Ratio of Increase of Ultimate Load for Composite Space Truss CT1 And CT2.

7. Conclusion

This study presents an experimental investigation on concrete-filled tubular steel members (CFST) as individual elements and as compression elements in space trusses. Individual CFST and hollow steel elements, as well as full composite and non-composite space trusses, were tested. The study discusses load capacity, deformed shape, and failure modes for CFST and steel members. A finite element study was carried out to model behavior during experimental work.
The following conclusions can be drawn from the results:

1. Filling steel tubes with concrete to form CFST members led to enhancements in behavior of compression members compared to hollow tubular steel members in terms of ultimate load capacity.
2. CFST and hollow steel members had the same deformed shape at the failure due to compression or brittle failure.
3. CFST members exhibited brittle behavior compared to hollow steel members.
4. The D/t ratio has a major effect on the behavior of CFST members; increasing D/t ratio leads to an increase in CFST capacity due to confinement pressure effect on concrete core.
5. Finite element modeling is capable of predicting ultimate load capacity and deformations for CFST and hollow steel members.

8. REFERENCES

[1] L. C. Schmidt, P. R. Morgan, and L. K. Stevens,"The influence of imperfections on the behaviour of a space truss", Second International Conference on Space Structures, University of Surrey, Billing & Sons Limited, UK, September 1975: pp 55-64, 1975.

[2] L. C. Schmidt, "Member buckling characteristics and space truss behaviour", lASS World Congress on Space Enclosures, Building Research Centre, Concordia University Montreal, July 1976: pp 849-857, 1975

[3] A. I. El-Sheikh and R. E. McConnel, “Experimental study of behavior of composite space trusses,” J. Struct. Eng. (United States), vol. 119, no. 3, pp. 747–766, 1993, doi: 10.1061/(ASCE)0733-9445(1993)119:3(747).

[4] A. Fülöp and M. Iványi, “Experimentally analyzed stability and ductility behaviour of a space-truss roof system,” Thin-Walled Struct., vol. 42, no. 2, pp. 309–320, 2004, doi: 10.1016/S0263-8231(03)00062-4.

[5] J. W. Kim, J. J. Kim, and H. J. Rhew, “Analysis and experiment for the formation and ultimate load testing of a hypar space truss,” J. Constr. Steel Res., vol. 62, no. 1–2, pp. 189–193, 2006, doi: 10.1016/j.jcsr.2005.04.020.

[6] Y. Sahol Hamid, P. Disney, and G. A. R. Parke, “Progressive Collapse of Double Layer Space Trusses,” Iabse-Iass Symp. London 2011, no. August 2011, 2015, doi: 10.13140/2.1.4215.2328.

[7] B. Young and E. Ellobody, “Experimental investigation of concrete-filled cold-formed high strength stainless steel tube columns,” J. Constr. Steel Res., vol. 62, no. 5, pp. 484–492, 2006, doi: 10.1016/j.jcsr.2005.08.004.

[8] E. Ellobody, “Nonlinear behavior of concrete-filled stainless steel stiffened slender tube columns,” Thin-Walled Struct., vol. 45, no. 3, pp. 259–273, 2007, doi: 10.1016/j.tws.2007.02.011.

[9] E. Ellobody, “Numerical modelling of fibre reinforced concrete-filled stainless steel tubular columns,” Thin-Walled Struct., vol. 63, pp. 1–12, 2013, doi: 10.1016/j.tws.2012.10.005.

[10] B. Uy, Z. Tao, and L. H. Han, “Behaviour of short and slender concrete-filled stainless steel tubular columns,” J. Constr. Steel Res., vol. 67, no. 3, pp. 360–378, 2011, doi: 10.1016/j.jcsr.2010.10.004.

[11] M. Dundu, “Column buckling tests of hot-rolled concrete filled square hollow sections of mild to high strength steel,” Eng. Struct., vol. 127, pp. 73–85, 2016, doi: 10.1016/j.engstruct.2016.08.039.

[12] M. Fong, S. L. Chan, and B. Uy, “Advanced design for trusses of steel and concrete-filled tubular sections,” Eng. Struct., vol. 33, no. 12,

pp. 3162–3171, 2011, doi: 10.1016/j.engstruct.2011.08.002.

[13] L. H. Han, W. Xu, S. H. He, and Z. Tao, "Flexural behaviour of concrete filled steel tubular (CFST) chord to hollow tubular brace truss: Experiments," J. Constr. Steel Res., vol. 109, pp. 137–151, 2015, doi: 10.1016/j.jcsr.2015.03.002.

[14] Y. Chen, R. Feng, and S. Gao, "Experimental study of concrete-filled multiplanar circular hollow section tubular trusses," Thin-Walled Struct., vol. 94, pp. 199–213, 2015, doi: 10.1016/j.tws.2015.04.013.

[15] ABAQUS Standard Us r's Manual 004 , Vol. 1 –3. Version 6.4. USA: Hibbitt, Karlsson and Sorensen Inc.

[16] Hu, H. ., S no ri W.C., "Constitutiv Mod ling of Con r t y Using Nonasso iat d Plasti ity", Journal of Materials in Civil Engineering , Vol. 1, No. 4, pp. 199 216, (1989).

[17] Mander JB, Priestley MJN, Park R. (1988), "Theoretical stress–strain model for confined concrete", Journal of Structural Engineering, ASCE, Vol. 114, No. 8, pp. 1804–1826.

[18] W. Zhou, Y. Chen, K. Wang, S. Han, and F. Palacios Galarza, "Experimental research on circular concrete filled stainless steel tubular truss," Thin-Walled Struct., vol. 117, no. April, pp. 224–238, 2017, doi:10.1016/j.tws.2017.04.026.

[19] "BUCKLING BEHAVIOR OF SQUARE-AND-DIAGONAL DOUBLE-LAYER GRID By Toshitsugu Saka ~ and Yoshiya Taniguchi 2," vol. 120, no. 4, pp. 1088–1102, 1994.

[20] A. El-Sheikh, "Development of a New Space Truss System," J. Constr. Steel Res., vol. 37, no. 3, pp. 205–227, 1996, doi: 10.1016/0143-974X(96)00004-1.

[21] A. El-Sheikh, "Failure mode and strength of space truss compression chord members," Eng. Struct., vol. 21, no. 5, pp. 395–405, 1999, doi: 10.1016/S0141-0296(97)00223-X.

[22] C. Vatansever, "Investigation of buckled truss bars of a space truss roof system," Eng. Fail. Anal., vol. 106, no. August 2016, p. 104156, 2019, doi: 10.1016/j.engfailanal.2019.104156.

[23] M. F. Hassanein, M. Elchalakani, and V. I. Patel, "Overall buckling behaviour of circular concrete-filled dual steel tubular columns with stainless steel external tubes," Thin-Walled Struct., vol. 115, no. July 2016, pp. 336–348, 2017, doi: 10.1016/j.tws.2017.01.035.

[24] W. Huang, Z. Lai, B. Chen, and P. Yao, "Experimental behavior and analysis of prestressed concrete-filled steel tube (CFT) truss girders," Eng. Struct., Vol. 152, pp. 607–618, 2017, doi: 10.1016/j.engstruct.2017.09.035.

[25] W. Huang, Z. Lai, B. Chen, Z. Xie, and A. H. Varma, "Concrete-filled steel tube (CFT) truss girders: Experimental tests, analysis, and design," Eng. Struct., Vol. 156, No. July 2017, pp. 118–129, 2018, doi: 10.1016/j.engstruct.2017.11.026.